

UC Riverside

2017 Publications

Title

More unsaturated, cooking-type hydrocarbon-like organic aerosol particle emissions from renewable diesel compared to ultra low sulfur diesel in at-sea operations of a research vessel

Permalink

<https://escholarship.org/uc/item/8j5970j7>

Journal

Aerosol Science and Technology, 51(2)

ISSN

0278-6826 1521-7388

Authors

Price, Derek J
Chen, Chia-Li
Russell, Lynn M
et al.

Publication Date

2017-01-13

DOI

10.1080/02786826.2016.1238033

Peer reviewed






More unsaturated, cooking-type hydrocarbon-like organic aerosol particle emissions from renewable diesel compared to ultra low sulfur diesel in at-sea operations of a research vessel

Derek J. Price, Chia-Li Chen, Lynn M. Russell, Maryam A. Lamjiri, Raghu Betha, Kevin Sanchez, Jun Liu, Alex K. Y. Lee & David R. Cocker


To cite this article: Derek J. Price, Chia-Li Chen, Lynn M. Russell, Maryam A. Lamjiri, Raghu Betha, Kevin Sanchez, Jun Liu, Alex K. Y. Lee & David R. Cocker (2017) More unsaturated, cooking-type hydrocarbon-like organic aerosol particle emissions from renewable diesel compared to ultra low sulfur diesel in at-sea operations of a research vessel, *Aerosol Science and Technology*, 51:2, 135-146, DOI: [10.1080/02786826.2016.1238033](https://doi.org/10.1080/02786826.2016.1238033)


To link to this article: <https://doi.org/10.1080/02786826.2016.1238033>

 [View supplementary material](#) 

 Accepted author version posted online: 20 Sep 2016.
Published online: 13 Jan 2017.

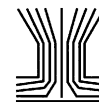
 [Submit your article to this journal](#) 

 Article views: 204

 [View related articles](#) 

 [View Crossmark data](#) 

 Citing articles: 3 [View citing articles](#) 



More unsaturated, cooking-type hydrocarbon-like organic aerosol particle emissions from renewable diesel compared to ultra low sulfur diesel in at-sea operations of a research vessel

Derek J. Price^a, Chia-Li Chen^a, Lynn M. Russell^a, Maryam A. Lamjiri^a, Raghu Betha^a, Kevin Sanchez^a, Jun Liu^a, Alex K. Y. Lee^b, and David R. Cocker^c

^aScripps Institution of Oceanography, University of California, San Diego, La Jolla, California, USA; ^bDepartment of Civil and Environmental Engineering, National University of Singapore, Singapore; ^cBourns College of Engineering, Center for Environmental Research and Technology, University of California—Riverside, Riverside, California, USA

ABSTRACT

The aerosol particle emissions from R/V *Robert Gordon Sproul* were measured during two 5-day research cruises (29 September–3 October 2014; 4–7 and 26–28 September 2015) at four engine speeds (1600 rpm, 1300 rpm, 1000 rpm, and 700 rpm) to characterize the emissions under different engine conditions for ultra low sulfur diesel (ULSD) and hydrogenation derived renewable diesel (HDRD) fuels. Organic aerosol composition and mass distribution were measured on the aft deck of the vessel directly behind the exhaust stack to intercept the ship plume. The ship emissions for both fuels were composed of alkane-like compounds ($H/C = 1.94 \pm 0.003$, $O/C = 0.04 \pm 0.001$, C_nH_{2n}) with mass spectral fragmentation patterns consistent with hydrocarbon-like organic aerosol (HOA). Single-particle mass spectra from emissions for both fuels showed two distinct HOA compositions, with one HOA type containing more saturated alkane fragments (C_nH_{2n+1}) and the other HOA type containing more monounsaturated fragments (C_nH_{2n-1}). The particles dominated by the C_nH_{2n-1} fragment series are similar to mass spectra previously associated with cooking emissions. More cooking-type organic particles were observed in the ship emissions for HDRD than for ULSD (45% and 38%, respectively). Changes in the plume aerosol composition due to photochemical aging in the atmosphere were also characterized. The higher fraction of alkene or aromatic (C_nH_{2n-m} , $m \geq 3$) fragments in aged compared to fresh plume emissions suggest that some of the semivolatile alkane-like components partition back to the vapor phase as dilution increases, while alkene or aromatic hydrocarbons contribute more mass to the particle phase due to continuing photochemical oxidation and subsequent condensation from the vapor phase.

ARTICLE HISTORY

Received 25 April 2016
Accepted 4 September 2016

EDITOR

Paul Ziemann

1. Introduction

Emissions from ocean going vessels are a significant contributor to atmospheric aerosol pollution. Aerosol and other pollutants from ship emissions have adverse effects on human health and the environment (Corbett et al. 2007; Deniz and Durmusoglu 2008). Large shipping ports, such as the Los Angeles and San Diego ports, are major pollution sources for their respective cities (Song 2014; Vutukuru and Dabdub 2008). Alternative shipping fuels that reduce net carbon emissions, including hydrogenation-derived renewable diesel (HDRD), are being investigated to understand how these fuels will change the chemical composition of atmospheric particles compared to emissions from ultra low sulfur diesel (ULSD).

To understand what chemical components are contributed by different sources of atmospheric particles, ambient aerosol measurements have used positive matrix factorization (PMF) analysis of aerosol mass spectrometer (AMS) measurements to apportion the organic components of atmospheric aerosol to different types of sources (Huang et al. 2010; Lanz et al. 2007; Liu et al. 2012; Mohr et al. 2012). Typical source-related factors identified by PMF of ambient AMS measurements include oxygenated organic aerosol (OOA), hydrocarbon-like organic aerosol (HOA), cooking organic aerosol (COA), and inorganic nitrate and sulfate (Allan et al. 2010; Zhang et al. 2005). HOA categories may sometimes include both the primary emissions of vehicles (m/z 43,

CONTACT Lynn M. Russell ✉ lmrussell@ucsd.edu Scripps Institution of Oceanography, University of California, San Diego, 9500 Gilman Drive, Mail Code 0221, La Jolla, CA 92093-0221, USA.

Color versions of one or more of the figures in the article can be found online at www.tandfonline.com/uast.

Supplemental data for this article can be accessed on the [publisher's website](#).

57, 71) and cooking (m/z 41, 55, 69) sources, but when separately quantified COA has been found to contribute 17–34% of the primary organic aerosol (Allan et al. 2010; Mohr et al. 2012). Contributions from different particle sources have also been identified by k -means clustering of single-particle measurements from ambient studies (Friedman et al. 2009; Lee et al. 2015; Liu et al. 2013; Rebotier and Prather 2007). While PMF is a powerful technique for determining the factors that contribute to the ensemble organic mass spectra, the k -means clustering analysis retains the number-based quantification by categorizing types of particles rather than splitting out the mass-based contributions to internal mixtures. Particle emissions from fuels derived from vegetable or animal oil feedstock are expected to have compositions with characteristics of both HOA and COA, but the specific chemical signatures of HDRD and ULSD for real-engine applications have not been investigated.

After emission into the atmosphere, the vapor and particle components of engine emissions continue to change due to dilution, cooling, and reactions in the atmosphere. The role of dilution and cooling on evaporating semivolatile components from particles has been characterized for fossil-fuel emissions (Robinson et al. 2010), showing that a substantial fraction of organic compounds that initially condense in concentrated plumes can evaporate because of dilution. The oxidation of individual fuel components (Nakao et al. 2012; Odum et al. 1996; Ziemann 2011) and the effects of photochemical aging on mixtures of organic components emitted from diesel engines (Chirico et al. 2010; Gordon et al. 2014; Nakao et al. 2011; Sage et al. 2008) have been investigated in smog chamber studies. Chirico et al. (2010) found that organic aerosol particles that were directly emitted from diesel engines were dominated by hydrocarbon compounds. While the fraction of oxygenated compounds increased after 5 h of photooxidation, these oxygenated compounds still contained large carbon chains that contributed to the hydrocarbon signal. There is little information, however, on the effects of photochemical aging of ship diesel emissions in actual light, temperature, and relative humidity conditions at the diluted concentrations typical of the atmosphere.

This study investigates the organic aerosol composition of the fresh (or direct) and aged emissions from a marine vessel operated on HDRD and ULSD. The combination of spectroscopic and spectrometric analyses of organic composition provides the most detailed characterization to date of the fuel-related differences in particle composition. The results also show the changes in chemical composition associated with photochemical formation of additional secondary components after emission into the atmosphere by comparing the freshly

emitted plume to the tracked aged plume. The analysis employs PMF and clustering to statistically separate the chemical characteristics of the particles emitted by the different fuels. This investigation provides the most comprehensive analysis to date of the organic composition of ship emissions, including their composition-based size distributions and the single-particle types. Two companion papers summarize (1) emission factors of CO, NO_x, number particle size distribution, and black carbon number and mass size distributions (Betha et al. 2017), and (2) reactive oxygen species formation and metal content of PM emissions (Kuang et al. 2017).

2. Methods

This work describes organic aerosol measurements of emissions from two sets of research cruises on the *R/V Robert Gordon Sproul*. The first set of detailed shipboard aerosol measurements was carried out from 29 September to 3 October in 2014 (2014 cruise). The second set of measurements was carried out from 4 to 7 September and from 26 to 28 September in 2015 (2015 cruise). These data are available at the UC San Diego library digital collections (Russell et al. 2016). Simultaneous measurements of stack gases and particle size distributions are described by Betha et al. (2017).

2.1. Vessel, engine, and fuel specifications

The *R/V Sproul* is a 355-ton, fixed-pitch twin-propeller oceanographic research vessel that has two main diesel engines and two auxiliary generators. The main diesel engine is a 2-stroke, 12-cylinder Detroit diesel 12V-149 engine. Two fuels, ultra low sulfur diesel (ULSD) and hydrogenation-derived renewable diesel (HDRD), were used to supply the diesel engines. The two fuels were kept in separate fuel tanks on the ship. To alternate between the two fuels, the valves on the fuel lines leading to the engine were switched. The fuel switch was performed in the evening and the engine was operated overnight to ensure the previous fuel was flushed from the fuel system before any engine cycle tests were conducted. The HDRD used in this study was NEXBTL, purchased from Neste Oil Corporation. Fuels were analyzed for C, H, O, and fatty acid methyl ester (FAME, COOR) content by Southwest Research Institute (San Antonio, TX, USA). Additional details about the engine and the fuel contents analysis results for both fuels are reported in Betha et al. (2017).

2.2. Aerosol sampling van instrumentation

Aerosol emissions from the *R/V Sproul* were measured using a suite of real-time instruments and off-line filter

analyses. The plume was sampled using an isokinetic inlet mounted on the sampling van. Sampled air was directed from the inlet to the suite of instruments housed in the van to measure the physicochemical properties of the plume aerosol. The chemical composition of the non-refractory components of the particle phase was measured by a high resolution—time of flight—aerosol mass spectrometer (HR-ToF-AMS, Aerodyne Research Inc., Billerica, MA, USA) after a PM₁ size-cut cyclone. Particles were also collected on Teflon filters after cyclone (PM₁) or impactor (PM_{0.18}) size cuts for off-line Fourier transform infrared (FTIR) spectroscopy. The CO₂ concentration measured at the sampling van was measured by a LI-840A CO₂/H₂O analyzer (LI-COR Environmental). Particle number concentration was measured by a condensation particle counter (CPC, model 3010, TSI Inc.). Additional instrumentation and measurements are reported by Betha et al. (2017) and Kuang et al. (2017).

The details of the HR-ToF-AMS have been described previously (DeCarlo et al. 2006; Jayne et al. 2000). The instrument was operated in two ion flight path modes. The shorter flight path (V-mode) provides better sensitivity at unit mass resolution (UMR), while the longer flight path (W-mode) provides sufficient mass spectral resolution (4300 at m/z 200) to determine empirical formulas of the ionized aerosol fragments. The fragmentation table coefficients used to estimate organic H₂O⁺ and CO⁺ signals are those presented in Aiken et al. (2008). The HR-ToF-AMS organic mass spectra were background subtracted to isolate the contribution of plume emissions. Background spectra were determined using an average of nonplume (marine ambient) conditions before and after plume sampling. The criteria for determining when sampling was considered to be in-plume include an increase in CO₂ concentration above background (Δ CO₂) of 10 ppm and peak HR-ToF-AMS size distribution mass concentrations above 2 $\mu\text{g m}^{-3}$ for fresh emissions. Organic aerosol during plume sampling was elevated above background by varying amounts based on engine speed, but generally the plume concentration was more than 2 $\mu\text{g m}^{-3}$ above the background, which is why this value was used as the threshold. The average organic concentration for the aged plume was 0.75 $\mu\text{g m}^{-3}$. A peak size distribution concentration threshold of 0.5 $\mu\text{g m}^{-3}$ was used for aged plume emissions as marine background was below that level. Due to the lack of sufficient measurements to quantify separately the differences expected in density and AMS collection efficiency (CE) for marine and plume aerosol particles, density and CE of 1.0 are reported in this study.

Characteristics of single particles were also investigated by the Event Trigger Single-Particle (ETSP) mode of the HR-ToF-AMS during the 2015 cruise. An event is

defined as a single mass spectrum (MS) extraction or series of consecutive extractions containing signals corresponding to the detection of a particle. The ETSP mode was set to have three regions of interest (ROI), which is a continuous range of mass-to-charge values having signals associated with particles of interest. ROI1 was set to m/z 43 (C₃H₇⁺, hydrocarbon particles) with an event trigger level of 2 ions/extraction, ROI2 was set to m/z 46 (NO₂⁺, nitrate particles) with an event trigger level of 1.5 ions/extraction, and ROI3 was set to m/z 48–150 (sulfate and organic particles) with an event trigger level of 4 ions/extraction. These regions of interest were selected to measure both the ship plume and marine ambient particles. Single-particle measurements were analyzed by Tofware version 2.5.3.b (developed by TOFWERK and Aerodyne Research, Inc.) and cluster analysis panel (CAP) version ETv1.2a (developed by Alex Lee and Megan Willis, National University of Singapore and University of Toronto). The HR-ToF-AMS was operated under a 5-min mode switching cycle (V-mode, 2-min; ETSP-mode (UMR), 2-min; W-mode, 1-min).

The organic functional groups of submicron atmospheric particles were measured using Fourier transform infrared (FTIR) spectroscopy. Atmospheric particles were sampled on 37-mm Teflon filters using a 1- μm sharp-cut cyclone at a flow rate of 16.7 lpm. Secondary Teflon filters placed in-line behind the sampling filters were used as a measure of sample contamination or artifacts and contained negligible organic mass. Samples were then frozen and transported to the laboratory for FTIR spectroscopy analysis. All samples were kept in a humidity- and temperature-controlled room (RH = 35–45%, Temp = 20°C) for at least 24 h prior to the analysis. Functional groups associated with carbon bond types, including alkane groups, alkene or aromatic groups, alcohol groups, carboxylic acid groups, carbonyl groups, and amine groups were characterized based on the absorbance of infrared wavelengths by each sample using Tensor 27 spectrometer (Bruker Optics). An automated algorithm including baselining, peak-fitting, and integration was used to interpret the FTIR spectrum from each filter (Russell et al. 2009; Takahama et al. 2013). The micromoles of alkene, aromatic, organonitrate, organosulfate, and carboxylic acid functional groups were below detection limit for all samples. The FTIR spectra are background-subtracted and normalized to air volume and CO₂ concentration.

2.3. Ship operations for aerosol sampling

During the 2014 and 2015 cruises, the chemical composition of the emissions were measured using the “plume intercept” method, i.e., by heading the bow of the ship

directly into the wind so that the stack emissions are blown aft into the inlet of the aerosol sampling van (Figure 1). Particles in the ship plume were measured approximately 20 m downwind of the vessel exhaust stack, with relative wind speeds of 2–20 m s⁻¹ providing 1–10 s for dilution and cooling before sampling by the van.

The “fresh” plume measurements are those measured traveling upwind so that the plume was diluted and cooled by mixing with ambient air but typically less than 10 s of mixing time in the atmosphere. The intercepted plume had temperatures indistinguishable from surrounding air but elevated CO₂, with measured CO₂ concentrations indicating dilution from stack conditions by factors ranging from 50 to 100. For the engine cycle sampling of fresh emissions, the ship engine was operated at constant engine speed, with 1-h operation each at 700, 1000, 1300, and 1600 rpm.

The “aged” plume was sampled by steaming crosswind for 10 min then turning approximately downwind to follow the plume. By approximately matching the

wind and ship heading, the crosswind 10-min track of emissions could be sampled nearly continuously for 1–3 h, similar to the E-PEACE measurements (Russell et al. 2013; Wonaschutz et al. 2013). Since the ship speed was slightly ahead of the wind, the current fresh emissions from the stacks were not intercepted by the sampling van. The criterion used to determine when the sampling inlet was considered to be in-plume was a particle concentration above 2000 cm⁻³, which was more than twice the background concentration of the surrounding air. To ensure that the ship remained in the plume, the CPC display was relayed to the bridge of the ship, allowing real-time course corrections.

3. Results and discussion

The overall organic aerosol mass concentrations of HDRD and ULSD emissions are similar, consistent with the similar elemental compositions and cetane indices of the fuels (Betha et al. 2017). The chemical composition and size differences between emissions for the two fuels are highlighted in the following sections.

3.1. Elemental ratios of organic particles from engine emissions

Atomic oxygen-to-carbon (O/C) ratios are a measure of the oxidation state of organic aerosol. Aiken et al. (2008) found that ambient urban O/C ranged from 0.2 to 0.8 with lower O/C for primary emissions while atomic hydrogen-to-carbon (H/C) ratios ranged from 1.4 to 1.9 with higher H/C for primary emissions. The elemental ratios indicate that during the times when the van was sampling ship engine emissions (for either HDRD or ULSD), the aerosol particle emissions consist of highly reduced organic components, consistent with fossil fuel hydrocarbons with very low fractions of oxygen or other heteroatoms (Aiken et al. 2008). Typically, the fresh ship emissions had elemental ratios of O/C = 0.04 ± 0.001 and H/C = 1.94 ± 0.003. Recent improvements to the HR-ToF-AMS fragmentation table corrections used for ambient elemental ratio analysis (Canagaratna et al. 2015) were applied to this dataset. The elemental ratios for the fresh ship emissions using the “improved ambient” method were O/C = 0.05 ± 0.002 and H/C = 2.10 ± 0.003. These metrics are consistent with most of the organic mass consisting of C_nH_{2n} molecules, which is a mixture of saturated alkanes (C_nH_{2n+1}) and monounsaturated alkenes or cyclic alkanes (C_nH_{2n-1}–C_nH_{2n-3}). A large number of the alkane groups are likely present in chain lengths of 23 or more carbons, since shorter hydrocarbons would preferentially remain in the vapor



Figure 1. Picture of the exhaust stacks of the R/V *Robert Gordon Sproull* with the ambient sampling van secured to the aft deck.

phase due to their higher vapor pressure (Fraser et al. 1997).

In contrast, the background, marine aerosol nonrefractory organic composition is more oxidized with more variability in the elemental ratios. Typically, the background aerosol had elemental ratios of $O/C = 0.5$ – 0.8 and $H/C = 1.2$ – 1.3 . During times of consistent plume or marine ambient sampling, the elemental ratios are constant. The elemental ratios change rapidly when the sampling inlet moves in and out of the plume. The time series of the elemental ratios over both cruises is shown in Figure S1 (see the online supplemental information [SI]).

3.2. Differences in particle organic composition with fuel type and engine speed

The organic mass spectra obtained by the HR-ToF-AMS for both fuels at different engine speeds are shown in Figure 2. Comparisons between the different spectra were obtained through linear regression analysis. Similarities between spectra were also calculated using the normalized dot product method (Marcolli et al. 2006). The spectra were normalized by dividing the m/z peak

intensities by the square root of the sum of the squares of the individual peak intensities. The normalized spectra then represent vectors. The dot product is the cosine of the angle between the two vectors. A value of 0 means the spectra are orthogonal, while a value of 1 means the spectra are identical. The linear regression equations, r^2 values, and dot product values for each comparison are summarized in Table 1. To better illustrate the variations between each of the fresh and aged spectra, the organic mass spectra were normalized to the total intensity and then subtracted from each other to form difference spectra (Figure 3).

The mass spectra are quite similar between each engine speed for both fuels (Figures 2a–d). The spectrum for fresh HDRD (700 rpm) correlates well with the fresh ULSD (700 rpm) spectrum ($r^2 = 0.998$; DP = 0.9990). This could be due to a similar chemical makeup between the two fuels. Additionally, it has been shown that lubricating oil can dominate emissions from motor vehicles (Worton et al. 2014). There is a small difference between HDRD and ULSD emissions, namely there is a more abundant hydrocarbon series in the ULSD mass spectra (m/z 43, 57, 71) (C_nH_{2n+1}) than in the HDRD mass spectra (m/z 41, 55, 69) (C_nH_{2n-1}). These differences are

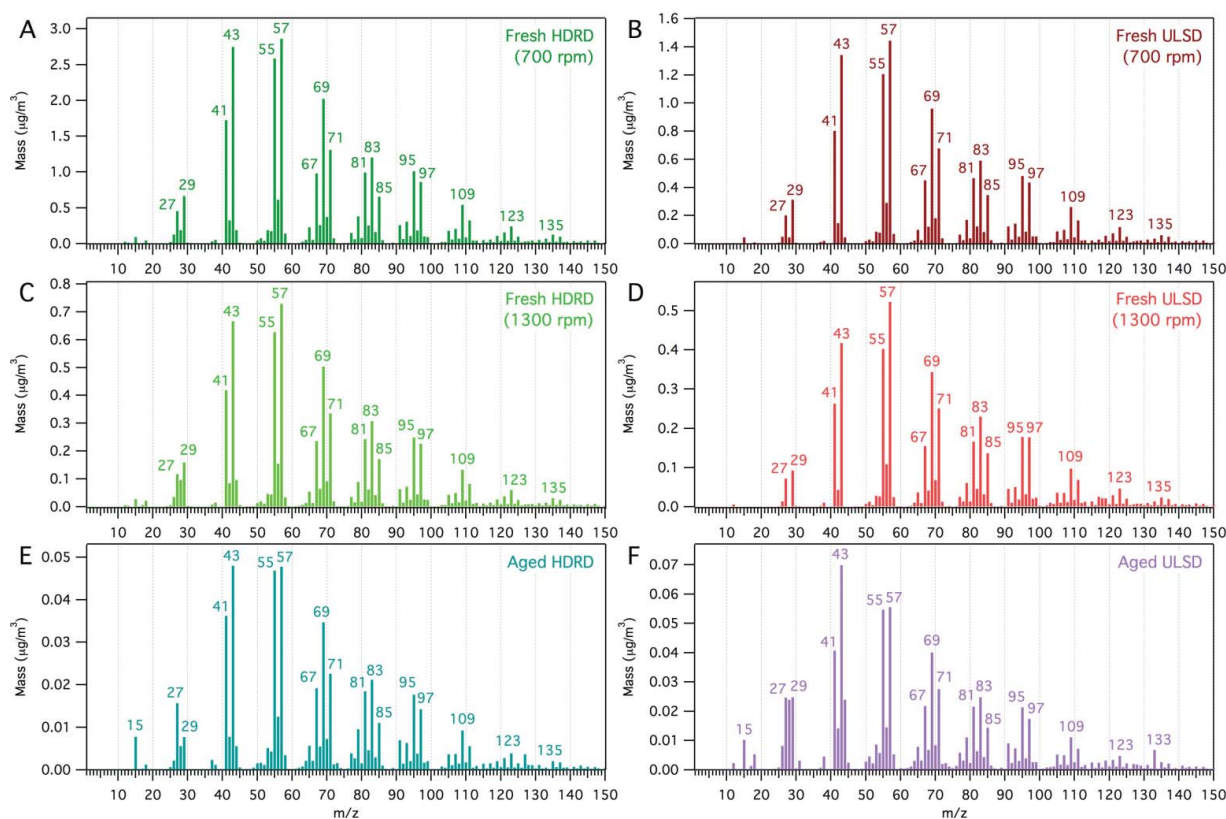


Figure 2. Background-subtracted HR-ToF-AMS organic mass spectra for fresh HDRD and ULSD emissions at 700 rpm engine speed (a–b), fresh HDRD and ULSD emissions at 1300 rpm engine speed (c–d), and aged HDRD and ULSD emissions (e–f). HR-ToF-AMS spectra from the 2015 cruise were used for the analysis.

Table 1. Summary of the linear regression and dot product analyses for the comparison of the HR-ToF-AMS organic mass spectra.

Mass Spectra Comparison	Linear Regression Equation	r^2 Value	Dot Product of Spectra
Fresh HDRD (700 rpm) vs. Fresh ULSD (700 rpm)	$y = 2.058x + 0.0004$	0.998	0.9990
Fresh HDRD (700 rpm) vs. Fresh HDRD (1300 rpm)	$y = 4.028x - 0.003$	0.997	0.9987
Fresh ULSD (700 rpm) vs. Fresh ULSD (1300 rpm)	$y = 2.866x - 0.001$	0.990	0.9956
Fresh HDRD (700 rpm) vs. Aged HDRD	$y = 55.497x - 0.016$	0.980	0.9909
Fresh ULSD (700 rpm) vs. Aged ULSD	$y = 20.314x - 0.016$	0.901	0.9545
Aged HDRD vs. Aged ULSD	$y = 0.761x - 0.000$	0.936	0.9725

more clearly seen in the difference spectrum (Figure 3a). At higher m/z (>80), there are a greater number of possible fragment ions contributing to each m/z , including cyclic fragments (C_6+). Therefore, the trends shift to less saturated fragments at higher m/z ($C_nH_{2n+1} \rightarrow C_nH_{2n-1}$ and $C_nH_{2n-1} \rightarrow C_nH_{2n-3}$).

The correlations between the 700 rpm and 1300 rpm engine speeds for both HDRD and ULSD (Table 1) show considerable similarity in the spectra ($r^2 = 0.997$ and 0.990 , respectively; dot product = 0.9987 and 0.9956 , respectively). The difference spectra between the 700 rpm and 1300 rpm engine speeds (Figures 3c and d) show more saturated n -alkane and branched alkane m/z peaks ($C_nH_{2n+1} - C_nH_{2n-1}$) in the 1300 rpm spectra and more cycloalkane m/z peaks in the 700 rpm spectra ($C_nH_{2n-1} - C_nH_{2n-3}$). This suggests a greater concentration of lubricating oil in the emissions at lower speed, as

lubricating oils have higher concentrations of cycloalkanes compared to fuel (Tobias et al. 2001). There is an increase in higher ($m/z > 55$) peaks at 1300 rpm compared to 700 rpm for ULSD. These results indicate a shift in concentration of the hydrocarbon components of the organic aerosol, consistent with higher relative amounts of longer chain hydrocarbons at the higher engine speed (1300 rpm) and more unburnt lubricating oil components at lower engine speed (700 rpm) (Cross et al. 2015).

Event trigger (ET) single-particle measurements were analyzed by a k -means clustering analysis using the cluster analysis panel (CAP) developed by Lee et al. (2015) in IGOR Pro (WaveMetrics Inc., Portland, OR, USA). Particles with dry vacuum aerodynamic diameters between 30 nm and 1000 nm with signal thresholds above 4.5 ions were defined as “real particles,” and

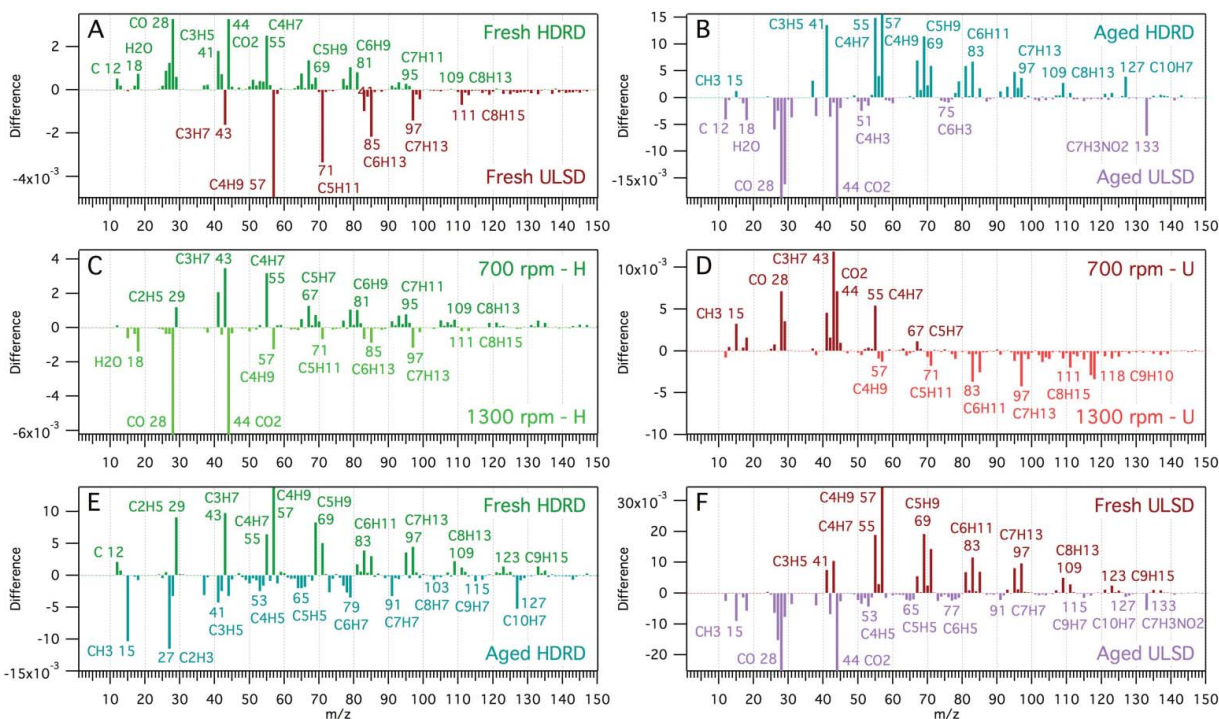


Figure 3. Difference spectra of the background-subtracted HR-ToF-AMS mass spectra (normalized to total intensity) between HDRD and ULSD emissions (a–b), emissions at 700 and 1300 rpm engine speeds for both fuels (c–d), and fresh and aged emissions for both fuels (e–f). The shift of greater m/z 28 and 44 (CO and CO_2 fragments) from 1300 rpm in HDRD to 700 rpm in ULSD is an artifact of background subtraction.

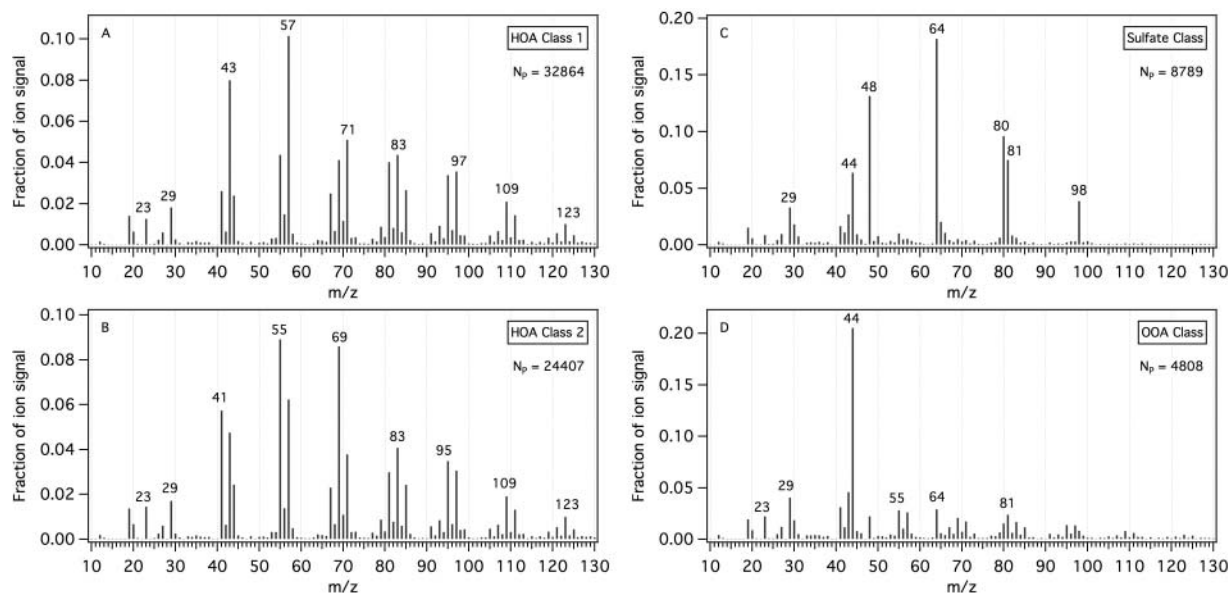


Figure 4. HR-ToF-AMS event trigger single-particle cluster mass spectra for the 2015 cruises. Four distinct particle classes were observed, including two hydrocarbon organic aerosol classes (a, b), a sulfate class (c), and an oxygenated organic aerosol class (d). The number of particles (N_p) for each particle class are shown.

particles below 30 nm or larger than 1000 nm were defined as background signal as shown in Figure S2. The measurements used for clustering included several HDRD and ULSD engine cycles as well as six 1-h marine background sampling times. The clustering solution with nine clusters (classes of particles) was determined to best fit the data set mathematically by minimizing the Euclidean distance between clusters (Figure S3; Lee et al. 2015). To provide physical meaning to the particle classes, some of the clusters needed to be recombined according to the procedure outlined in Lee et al. (2015), resulting in four distinct particle classes in this study.

The single-particle mass spectra and number of particles in each class are shown in Figure 4. Two of the particle classes have compositions similar to hydrocarbon-like organic aerosol (HOA, Zhang et al. [2011], Figures 4a and b). HOA class 1 is dominated by C_nH_{2n+1} fragment ions (m/z 43, 57, 71) consistent with diesel vehicle emissions, while HOA class 2 is dominated by C_nH_{2n-1} fragment ions (m/z 41, 55, 69), which are typically observed in cooking emissions (Mohr et al. 2009). The final two particle classes (Figures 4c and d) include a sulfate class (m/z 48, 64, 80, 81, 98) and an oxygenated organic aerosol (OOA) class (m/z 44), both of which were present in the marine background aerosol measured outside of the plume. The fraction of diesel-like HOA particles (class 1) is greater than the fraction of cooking-like HOA (class 2) for both fuels. However, the fraction of the cooking-like HOA (class 2) particles is greater in the HDRD emissions ($44.5 \pm 1.6\%$) than in the ULSD

emissions ($37.7 \pm 1.4\%$). This is consistent with the results observed in the organic mass spectra difference plots (Figure 3a). While the differences are modest, they are statistically different (Result of t -test assuming equal variances: t -statistic (2.078) > t -critical two-tail (2.073) at 95% confidence level). Since HDRD uses vegetable and animal oils as feedstock, the similarity of its particles to cooking-like particles is expected (He et al. 2004; Mohr et al. 2009). The single-particle analysis provides a way to track the relative contributions of these cooking-type components in the particle emissions.

For comparison purposes, positive matrix factorization (PMF) was applied to the high-resolution organic mass spectral data. Generally, PMF agreed well with the k -means clustering results. Three organic factors were separated with the PMF analysis, including two HOA factors and one OOA factor. The OOA factor correlated well with the clustering OOA class ($r^2 = 0.850$). The HOA factor 1 contained the C_nH_{2n+1} hydrocarbon series and correlated well with the clustering HOA class 1 ($r^2 = 0.866$). The HOA factor 2 contained the C_nH_{2n-1} hydrocarbon series and although the lower m/z (<70) correlated well with the clustering HOA class 2, the higher m/z shifted to more unsaturated hydrocarbon peaks which lowered the overall correlation ($r^2 = 0.413$). The ability of PMF and k -means clustering to distinguish two chemical components indicates a chemically heterogeneous mixture within the ship emissions.

Applying single-particle cluster analysis to individual engine cycles provides the fraction of particles in each



Figure 5. HR-ToF-AMS event trigger single-particle cluster analysis results for HDRD and ULSD emissions at 700, 1000, 1300, and 1600 rpm engine speeds as well as aged emissions, and marine background. The bars indicate the fraction of each identified particle class to the measured particle number. Four complete engine cycles (700–1600 rpm) were averaged for HDRD with whiskers showing the variability between cycles for each fraction. One complete engine cycle is shown for ULSD. The aged plume tests were divided into 1-h measurements (HDRD–4 h, ULSD–2 h). Marine ambient is the average of six separate 1-h marine background measurements. Individual measurement results are provided in Figure S4 in the SI. ET collection efficiency (CE) is likely particle-type-dependent. Therefore, the results are not CE-corrected.

class for each engine speed (Figure 5) and shows the differences in the hydrocarbon composition between the two fuels. There is consistently a greater fraction of cooking-type HOA (class 2) in the HDRD emissions than in the ULSD emissions at all speeds. For the engine cycles, the fraction of total particles with HOA-like composition

decreases with increasing speed. At higher speeds, more marine-background-type particles are observed mixed with plume particles, likely the result of the faster relative speed of the vessel making it more difficult to continuously intercept the plume for the 2-min duration of each AMS measurement. The repeatability of particle-type

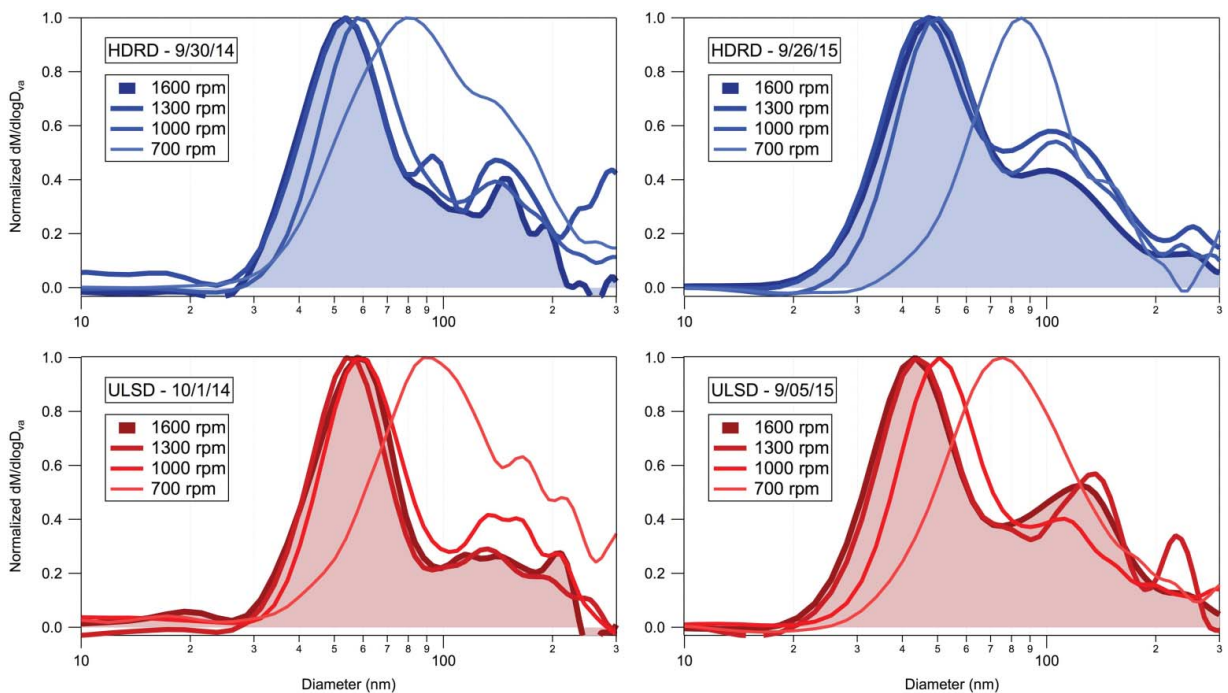


Figure 6. HR-ToF-AMS organic aerosol size distribution profiles for HDRD (9/30/14 and 9/26/15) and ULSD (10/1/14 and 9/5/15) emissions at different engine speeds. (Five-pass binomial smoothing was applied to the size distribution data.)

distribution at each engine speed over multiple HDRD engine cycles confirms the trend of decreasing HOA particles with increasing engine speed.

Small differences in the mass spectra are consistent with small differences in the size distributions of the organic mass concentrations at different engine speeds (Figure 6). Two size modes are observed at 1000, 1300, and 1600 rpm, and there is an increase of the mean diameter of the smaller organic particle mode with decreasing engine speed (45 nm at 1600 rpm to 80 nm at 700 rpm). The second size mode remains at ~ 100 nm for HDRD and ~ 130 nm for ULSD. At the lowest engine speed (700 rpm), the smaller size mode may be indistinguishable from the second size mode. The shift in small-particle mode to larger diameters and lack of separate small-particle mode at lower engine speeds is consistent with particle mobility size distributions reported in Betha et al. (2017). These observed differences in size distribution were consistent for all of the engine cycles for HDRD and ULSD.

FTIR spectra for plume emissions are shown in Figure 7. The plume samples show two distinct hydrocarbon peaks at $2800\text{--}3000\text{ cm}^{-1}$ for all engine speeds and fuels. These absorption peaks are due to C–H stretching in methyl and methylene groups (Stuart 2004), and the sharp and parallel double peaks are

consistent with hydrocarbon chains longer than ten carbons. For the HDRD cycle, the hydrocarbon peak absorbance increases with decreasing speed. The ULSD cycle follows the same trend with the exception of the 700 rpm sample. The ratio between the two methylene peaks at 2850 and 2930 cm^{-1} in the HDRD cycles is very consistent for fresh emissions at all speeds at 1.65. The ratio is slightly greater for the ULSD emissions at 1.85, consistent with small differences in the alkane carbon number distribution of the two fuel emissions.

3.3. Changes in particle organic composition with plume aging

The organic mass spectra from the aged emissions of HDRD and ULSD (Figures 2e and f) appear similar to the fresh emissions. There is a good correlation (Table 1) between the fresh (700 rpm) spectra and the aged emissions spectra for both HDRD and ULSD ($r^2 = 0.980$ and 0.901 , respectively; dot product = 0.9909 and 0.9545 , respectively) indicating only slight changes in chemical composition after the 1–4 h of atmospheric aging. The difference spectra (Figures 3e and f) show that the aged emissions of HDRD and ULSD contain higher relative amounts of alkene or aromatic fragments (C_nH_{2n-3} to C_nH_{2n-13}) (Canagaratna et al. 2004; Chirico et al. 2010)

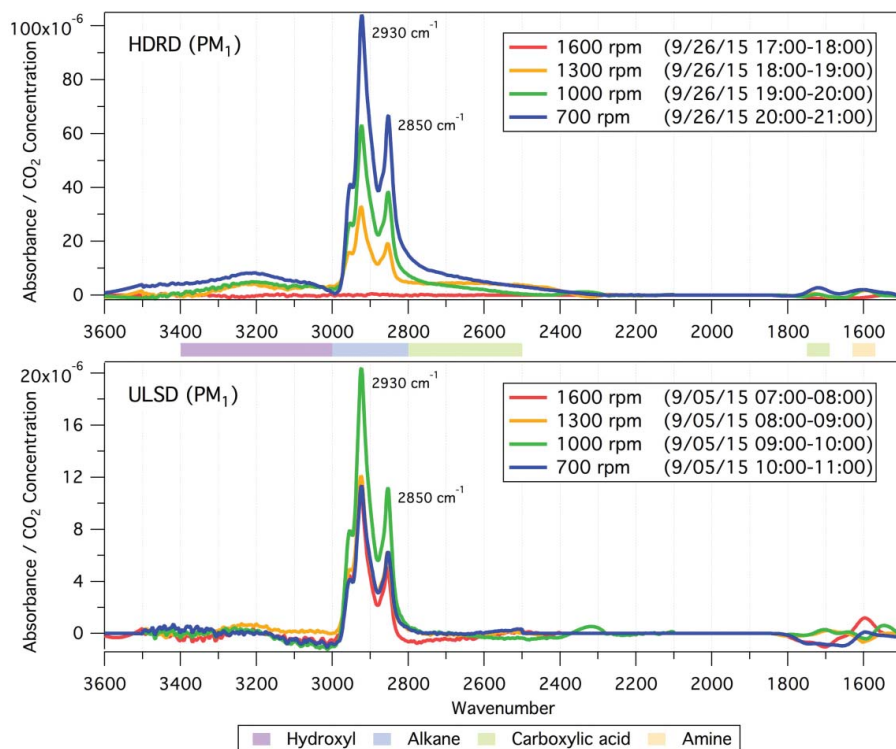


Figure 7. FTIR spectra (background subtracted and normalized to CO_2 concentration) for PM_{10} size cutoff samples of HDRD (9/26/15) and ULSD (9/5/15) emissions at 700, 1000, 1300, and 1600 rpm engine speeds. Shaded areas denote absorption peak locations for different functional groups.

compared to the fresh emissions, which contain higher relative amounts of saturated alkane, cycloalkane, and monounsaturated alkene fragment ions (C_nH_{2n+1} to C_nH_{2n-3}). This increase in aromatic fragments with aging is seen for both the aged HDRD and aged ULSD, although there is slightly more hydrocarbon-like aerosol in the aged HDRD emissions compared to the ULSD emissions (Figure 3b). One explanation for the reduction in the relative number of alkane groups is that as the plume is diluted further, with in-plume ΔCO_2 being twice as large in the fresh plume compared to the aged plume, the gas to particle equilibrium shifts some of the semi-volatile alkane hydrocarbons back to the gas phase. Simultaneous to this dilution and phase partitioning effect, unsaturated and polycyclic aromatic hydrocarbons (PAH) in the vapor phase emissions may oxidize to form lower vapor pressure compounds that partition to the particle phase. The combined result of the decrease in saturated hydrocarbons due to evaporation and increase in alkene or aromatic fragments due to photochemical oxidation could explain the observed result. The possible reduction in alkane groups by heterogeneous oxidation on the particles was ruled out due to the short time (1–4 h) available in the atmosphere (Kroll et al. 2015).

The single-particle cluster analysis (Figure 5) confirms that the combination of dilution and chemical reactions reduced the HOA classes from about 90% of the total particle number in the fresh 700 rpm emissions to only 30–40% of the total particle number in the aged emissions. The remaining 60–70% of the particle number was composed of sulfate and OOA class particles from the marine background. The cluster analysis (nine-cluster solution) did not separate out the HOA class-2 in the aged HDRD tests. This low particle count for HOA class-2 relative to HOA class-1 likely results from removal of class 2 by atmospheric processes (dilution/reaction) during aging.

4. Summary

The organic chemical composition of aerosol particles from ULSD and HDRD emissions are similar. This could be due to a similar chemical makeup between fuels in addition to a large contribution from lubricating oil. The HR-ToF-AMS mass spectra contain hydrocarbon fragmentation patterns (m/z 41, 43, 55, 57, 69, 71, 83, 85, 95, 97, and 109), the FTIR spectra show sharp hydrocarbon peaks at 2800–3000 wavenumbers, and in-plume HR-ToF-AMS elemental ratios are consistent with C_nH_{2n} fragments ($H/C = 1.94 \pm 0.003$, $O/C = 0.04 \pm 0.001$), which indicates the ship exhaust is mainly composed of alkane-like hydrocarbons. There were small differences observed in the HR-ToF-AMS mass spectra and FTIR

absorbance spectra between the two fuels. The HR-ToF-AMS single-particle mass spectra showed two HOA-like particles (diesel-type HOA class 1 = m/z 43, 57, 71, and cooking-type HOA class 2 = m/z 41, 55, 69). The cooking-type HOA (class 2) particles were more abundant in the HDRD emissions than in the ULSD emissions.

The hydrocarbon peak ratio in the FTIR spectra was slightly different between HDRD and ULSD emissions (1.65 and 1.85, respectively), likely resulting from differences in the carbon number distribution of hydrocarbons in the two fuels. The HR-ToF-AMS particle size distribution showed smaller particle diameters for HDRD compared to ULSD, with both fuels showing changes in particle sizes for different engine speeds. In general, particle diameter increased with decreasing engine speed, but this trend was more consistent for ULSD than HDRD.

The comparison of fresh and aged HR-ToF-AMS spectra shows that aged particles had a higher ratio of aromatic to alkane fragments for both HDRD and ULSD. For example, the ratio of m/z 53 (C_4H_5) to m/z 57 (C_4H_9) was 25% higher in aged plumes compared to fresh emissions. The increase in the relative number of aromatic groups (or equivalently the decrease in the relative number of alkane groups) suggests that aromatic fragments condensed from the vapor to particles after the fresh emissions were measured, requiring additional time for oxidation to form lower volatility compounds. Dilution of the plume during aging may have shifted some of the semivolatile alkane hydrocarbons back to the gas phase. Further studies are needed to specifically identify the processes involved in aging and to better assess the robustness of these results in different conditions.

Acknowledgments

The authors would like to thank Bruce Applegate, Sujit Ghosh, and the crew of the R/V *Robert Gordon Sproul*, including Captain Christopher Welton, Ernie Bayer, Paul Mauricio, and Bud Hale for their assistance. The authors also acknowledge the instrumentation and personnel contributions from the University of California Riverside (Xinze Peng) and the University of California Los Angeles (Xiaobi M. Kuang and Gisele O. da Rocha).

Funding

Funding for this study was provided by the Department of Transportation Grant DTMA-91-H-2013-0001.

ORCID

Derek J. Price  <http://orcid.org/0000-0003-3693-1475>
Lynn M. Russell  <http://orcid.org/0000-0002-6108-2375>

References

- Aiken, A. C., Decarlo, P. F., Kroll, J. H., Worsnop, D. R., Huffman, J. A., Docherty, K. S., Ulbrich, I. M., Mohr, C., Kimmel, J. R., Sueper, D., Sun, Y., Zhang, Q., Trimborn, A., Northway, M., Ziemann, P. J., Canagaratna, M. R., Onasch, T. B., Alfarra, M. R., Prevot, A. S. H., Dommen, J., Duplissy, J., Metzger, A., Baltensperger, U., and Jimenez, J. L. (2008). O/C and OM/OC Ratios of Primary, Secondary, and Ambient Organic Aerosols with High-Resolution Time-of-Flight Aerosol Mass Spectrometry. *Environ. Sci. Technol.*, 42:4478–4485.
- Allan, J. D., Williams, P. I., Morgan, W. T., Martin, C. L., Flynn, M. J., Lee, J., Nemitz, E., Phillips, G. J., Gallagher, M. W., and Coe, H. (2010). Contributions from Transport, Solid Fuel Burning and Cooking to Primary Organic Aerosols in two UK Cities. *Atmos. Chem. Phys.*, 10:647–668.
- Betha, R., Russell, L. M., Sanchez, K., Liu, J., Price, D. J., Lamjiri, M. A., Chen, C., Kuang, X. M., da Rocha, G. O., Paulson, S. E., Miller, J. W., and Cocker, D. R. (2017). Lower NO_x but Higher Particle and Black Carbon Emissions from Renewable Diesel Compared to Ultra Low Sulfur Diesel in At-Sea Operations of a Research Vessel. *Aerosol Sci. Technol.*, 51(2):123–134.
- Canagaratna, M. R., Jayne, J. T., Ghertner, D. A., Herndon, S., Shi, Q., Jimenez, J. L., Silva, P. J., Williams, P., Lanni, T., Drewnick, F., Demerjian, K. L., Kolb, C. E., and Worsnop, D. R. (2004). Chase Studies of Particulate Emissions from in-use New York City Vehicles. *Aerosol Sci. Technol.*, 38:555–573.
- Canagaratna, M. R., Jimenez, J. L., Kroll, J. H., Chen, Q., Kessler, S. H., Massoli, P., Ruiz, L. H., Fortner, E., Williams, L. R., Wilson, K. R., Surratt, J. D., Donahue, N. M., Jayne, J. T., and Worsnop, D. R. (2015). Elemental Ratio Measurements of Organic Compounds Using Aerosol Mass Spectrometry: Characterization, Improved Calibration, and Implications. *Atmos. Chem. Phys.*, 15:253–272.
- Chirico, R., DeCarlo, P. F., Heringa, M. F., Tritscher, T., Richter, R., Prevot, A. S. H., Dommen, J., Weingartner, E., Wehrle, G., Gysel, M., Laborde, M., and Baltensperger, U. (2010). Impact of Aftertreatment Devices on Primary Emissions and Secondary Organic Aerosol Formation Potential from in-use Diesel Vehicles: Results from Smog Chamber Experiments. *Atmos. Chem. Phys.*, 10:11545–11563.
- Corbett, J. J., Winebrake, J. J., Green, E. H., Kasibhatla, P., Eyring, V., and Lauer, A. (2007). Mortality from Ship Emissions: A Global Assessment. *Environ. Sci. Technol.*, 41:8512–8518.
- Cross, E. S., Sappok, A. G., Wong, V. W., and Kroll, J. H. (2015). Load-Dependent Emission Factors and Chemical Characteristics of IVOCs from a Medium-Duty Diesel Engine. *Environ. Sci. Technol.*, 49:13483–13491.
- DeCarlo, P. F., Kimmel, J. R., Trimborn, A., Northway, M. J., Jayne, J. T., Aiken, A. C., Gonin, M., Fuhrer, K., Horvath, T., Docherty, K. S., Worsnop, D. R., and Jimenez, J. L. (2006). Field-Deployable, High-Resolution, Time-of-Flight Aerosol Mass Spectrometer. *Anal. Chem.*, 78:8281–8289.
- Deniz, C., and Durmusoglu, Y. (2008). Estimating Shipping Emissions in the Region of the Sea of Marmara, Turkey. *Sci. Total Environ.*, 390:255–261.
- Fraser, M. P., Cass, G. R., Simoneit, B. R. T., and Rasmussen, R. A. (1997). Air quality Model Evaluation Data for Organics .4. C-2-C-36 non-Aromatic Hydrocarbons. *Environ. Sci. Technol.*, 31:2356–2367.
- Friedman, B., Herich, H., Kammermann, L., Gross, D. S., Arneth, A., Holst, T., and Cziczko, D. J. (2009). Subarctic Atmospheric Aerosol Composition: 1. Ambient Aerosol Characterization. *J. Geophys. Res.—Atmos.*, 114, D13203.
- Gordon, T. D., Presto, A. A., Nguyen, N. T., Robertson, W. H., Na, K., Sahay, K. N., Zhang, M., Maddox, C., Rieger, P., Chattopadhyay, S., Maldonado, H., Maricq, M. M., and Robinson, A. L. (2014). Secondary Organic Aerosol Production from Diesel Vehicle Exhaust: Impact of Aftertreatment, Fuel Chemistry and Driving Cycle. *Atmos. Chem. Phys.*, 14:4643–4659.
- He, L. Y., Hu, M., Huang, X. F., Yu, B. D., Zhang, Y. H., and Liu, D. Q. (2004). Measurement of Emissions of Fine Particulate Organic Matter from Chinese Cooking. *Atmos. Environ.*, 38:6557–6564.
- Huang, X. F., He, L. Y., Hu, M., Canagaratna, M. R., Sun, Y., Zhang, Q., Zhu, T., Xue, L., Zeng, L. W., Liu, X. G., Zhang, Y. H., Jayne, J. T., Ng, N. L., and Worsnop, D. R. (2010). Highly Time-Resolved Chemical Characterization of Atmospheric Submicron Particles During 2008 Beijing Olympic Games Using an Aerodyne High-Resolution Aerosol Mass Spectrometer. *Atmos. Chem. Phys.*, 10:8933–8945.
- Jayne, J. T., Leard, D. C., Zhang, X. F., Davidovits, P., Smith, K. A., Kolb, C. E., and Worsnop, D. R. (2000). Development of an Aerosol Mass Spectrometer for Size and Composition Analysis of Submicron Particles. *Aerosol Sci. Technol.*, 33:49–70.
- Kroll, J. H., Lim, C. Y., Kessler, S. H., and Wilson, K. R. (2015). Heterogeneous Oxidation of Atmospheric Organic Aerosol: Kinetics of Changes to the Amount and Oxidation State of Particle-Phase Organic Carbon. *J. Phys. Chem. A*, 119:10767–10783.
- Kuang, X. M., Scott, J. A., da Rocha, G. O., Betha, R., Price, D. J., Russell, L. M., Cocker, D. R., and Paulson, S. E. (2017). Hydroxyl Radical Formation and Trace Metal Content in Particulate Matter from Renewable Diesel and Ultra Low Sulfur Diesel in At-Sea Operations of a Research Vessel. *Aerosol Sci. Technol.*, 51(2):147–158.
- Lanz, V. A., Alfarra, M. R., Baltensperger, U., Buchmann, B., Hueglin, C., and Prevot, A. S. H. (2007). Source Apportionment of Submicron Organic Aerosols at an Urban Site by Factor Analytical Modelling of Aerosol Mass Spectra. *Atmos. Chem. Phys.*, 7:1503–1522.
- Lee, A. K. Y., Willis, M. D., Healy, R. M., Onasch, T. B., and Abbatt, J. P. D. (2015). Mixing State of Carbonaceous Aerosol in an Urban Environment: Single Particle Characterization Using the Soot Particle Aerosol Mass Spectrometer (SP-AMS). *Atmos. Chem. Phys.*, 15:1823–1841.
- Liu, S., Ahlm, L., Day, D. A., Russell, L. M., Zhao, Y. L., Gentner, D. R., Weber, R. J., Goldstein, A. H., Jaoui, M., Offenberg, J. H., Kleindienst, T. E., Rubitschun, C., Surratt, J. D., Sheesley, R. J., and Scheller, S. (2012). Secondary Organic Aerosol Formation from Fossil Fuel Sources Contribute Majority of Summertime Organic Mass at Bakersfield. *J. Geophys. Res.—Atmos.*, 117, D00V26.
- Liu, S., Russell, L. M., Sueper, D. T., and Onasch, T. B. (2013). Organic Particle Types by Single-Particle Measurements Using a Time-of-Flight Aerosol Mass Spectrometer Coupled with a Light Scattering Module. *Atmos. Meas. Tech.*, 6:187–197.

- Marcolli, C., Canagaratna, M. R., Worsnop, D. R., Bahreini, R., de Gouw, J. A., Warneke, C., Goldan, P. D., Kuster, W. C., Williams, E. J., Lerner, B. M., Roberts, J. M., Meagher, J. F., Fehsenfeld, F. C., Marchewka, M., Bertman, S. B., and Middlebrook, A. M. (2006). Cluster Analysis of the Organic Peaks in Bulk Mass Spectra Obtained During the 2002 New England Air Quality Study with an Aerodyne Aerosol Mass Spectrometer. *Atmos. Chem. Phys.*, 6:5649–5666.
- Mohr, C., DeCarlo, P. F., Heringa, M. F., Chirico, R., Slowik, J. G., Richter, R., Reche, C., Alastuey, A., Querol, X., Seco, R., Penuelas, J., Jimenez, J. L., Crippa, M., Zimmermann, R., Baltensperger, U., and Prevot, A. S. H. (2012). Identification and Quantification of Organic Aerosol from Cooking and Other Sources in Barcelona Using Aerosol Mass Spectrometer Data. *Atmos. Chem. Phys.*, 12:1649–1665.
- Mohr, C., Huffman, J. A., Cubison, M. J., Aiken, A. C., Docherty, K. S., Kimmel, J. R., Ulbrich, I. M., Hannigan, M., and Jimenez, J. L. (2009). Characterization of Primary Organic Aerosol Emissions from Meat Cooking, Trash Burning, and Motor Vehicles with High-Resolution Aerosol Mass Spectrometry and Comparison with Ambient and Chamber Observations. *Environ. Sci. Technol.*, 43:2443–2449.
- Nakao, S., Liu, Y., Tang, P., Chen, C. L., Zhang, J., and Cocker, D. R. (2012). Chamber Studies of SOA Formation from Aromatic Hydrocarbons: Observation of Limited Glyoxal Uptake. *Atmos. Chem. Phys.*, 12:3927–3937.
- Nakao, S., Shrivastava, M., Nguyen, A., Jung, H. J., and Cocker, D. (2011). Interpretation of Secondary Organic Aerosol Formation from Diesel Exhaust Photooxidation in an Environmental Chamber. *Aerosol. Sci. Technol.*, 45:964–972.
- Odum, J. R., Hoffmann, T., Bowman, F., Collins, D., Flagan, R. C., and Seinfeld, J. H. (1996). Gas/Particle Partitioning and Secondary Organic Aerosol Yields. *Environ. Sci. Technol.*, 30:2580–2585.
- Rebotier, T. P., and Prather, K. A. (2007). Aerosol Time-of-Flight Mass Spectrometry Data Analysis: A Benchmark of Clustering Algorithms. *Anal. Chim. Acta.*, 585:38–54.
- Robinson, A. L., Grieshop, A. P., Donahue, N. M., and Hunt, S. W. (2010). Updating the Conceptual Model for Fine Particle Mass Emissions from Combustion Systems. *J. Air Waste Manage.*, 60:1204–1222.
- Russell, L. M., Bahadur, R., Hawkins, L. N., Allan, J., Baumgardner, D., Quinn, P. K., and Bates, T. S. (2009). Organic Aerosol Characterization by Complementary Measurements of Chemical Bonds and Molecular Fragments. *Atmos. Environ.*, 43:6100–6105.
- Russell, L. M., Sorooshian, A., Seinfeld, J. H., Albrecht, B. A., Nenes, A., Ahlm, L., Chen, Y. C., Coggon, M., Craven, J. S., Flagan, R. C., Frossard, A. A., Jonsson, H., Jung, E., Lin, J. J., Metcalf, A. R., Modini, R., Mulmenstadt, J., Roberts, G. C., Shingler, T., Song, S., Wang, Z., and Wonaschutz, A. (2013). Eastern Pacific Emitted Aerosol Cloud Experiment. *Bull. Am. Meteorol. Soc.*, 94:709–729.
- Russell, L. M., Betha, R., Sanchez, K. J., Liu, J., Price, D. J., Lamjiri, M. A., Chen, C., Miller, J. W., and Cocker, D. R. (2016). Stack Gas and Plume Aerosol Measurements from Renewable Diesel and Ultra Low Sulfur Diesel in At-Sea Operation of Research Vessel Robert Gordon Sproul. UC San Diego Library Digital Collections. Available at <http://doi.org/10.6075/J0V985ZZ>
- Sage, A. M., Weitkamp, E. A., Robinson, A. L., and Donahue, N. M. (2008). Evolving Mass Spectra of the Oxidized Component of Organic Aerosol: Results from Aerosol Mass Spectrometer Analyses of Aged Diesel Emissions. *Atmos. Chem. Phys.*, 8:1139–1152.
- Song, S. (2014). Ship Emissions Inventory, Social Cost and Eco-Efficiency in Shanghai Yangshan Port. *Atmos. Environ.*, 82:288–297.
- Stuart, B. H. (2004). *Infrared Spectroscopy: Fundamentals and Applications*. John Wiley & Sons, Ltd, West Sussex.
- Takahama, S., Johnson, A., and Russell, L. M. (2013). Quantification of Carboxylic and Carbonyl Functional Groups in Organic Aerosol Infrared Absorbance Spectra. *Aerosol. Sci. Technol.*, 47:310–325.
- Tobias, H. J., Beving, D. E., Ziemann, P. J., Sakurai, H., Zuk, M., McMurry, P. H., Zarling, D., Waytulonis, R., and Kittelson, D. B. (2001). Chemical Analysis of Diesel Engine Nanoparticles Using a Nano-DMA/Thermal Desorption Particle Beam Mass Spectrometer. *Environ. Sci. Technol.*, 35:2233–2243.
- Vutukuru, S., and Dabdub, D. (2008). Modeling the Effects of Ship Emissions on Coastal Air Quality: A Case Study of Southern California. *Atmos. Environ.*, 42:3751–3764.
- Wonaschutz, A., Coggon, M., Sorooshian, A., Modini, R., Frossard, A. A., Ahlm, L., Mulmenstadt, J., Roberts, G. C., Russell, L. M., Dey, S., Brechtel, F. J., and Seinfeld, J. H. (2013). Hygroscopic Properties of Smoke-Generated Organic Aerosol Particles Emitted in the Marine Atmosphere. *Atmos. Chem. Phys.*, 13:9819–9835.
- Worton, D. R., Isaacman, G., Gentner, D. R., Dallmann, T. R., Chan, A. W. H., Ruehl, C., Kirchstetter, T. W., Wilson, K. R., Harley, R. A., and Goldstein, A. H. (2014). Lubricating Oil Dominates Primary Organic Aerosol Emissions from Motor Vehicles. *Environ. Sci. Technol.*, 48:3698–3706.
- Zhang, Q., Alfarra, M. R., Worsnop, D. R., Allan, J. D., Coe, H., Canagaratna, M. R., and Jimenez, J. L. (2005). Deconvolution and Quantification of Hydrocarbon-Like and Oxygenated Organic Aerosols Based on Aerosol Mass Spectrometry. *Environ. Sci. Technol.*, 39:4938–4952.
- Zhang, Q., Jimenez, J. L., Canagaratna, M. R., Ulbrich, I. M., Ng, N. L., Worsnop, D. R., and Sun, Y. L. (2011). Understanding Atmospheric Organic Aerosols Via Factor Analysis of Aerosol Mass Spectrometry: A Review. *Anal. Bioanal. Chem.*, 401:3045–3067.
- Ziemann, P. J. (2011). Effects of Molecular Structure on the Chemistry of Aerosol Formation from the OH-Radical-Initiated Oxidation of Alkanes and Alkenes. *Int. Rev. Phys. Chem.*, 30:161–195.